Journal of Alloys and Compounds 509 (2011) 5376–5380

Contents lists available at ScienceDirect

Journal of Alloys and Compounds

journal homepage: www.elsevier.com/locate/jallcom

Corrosion behavior of shape memory stainless steel in acid media

C.A. Della Rovere[a,*], J.H. Alano[a], J. Otubo[b], S.E. Kuri[a]

[a] Department of Materials Engineering, Federal University of São Carlos, Rodovia Washington Luis, Km 235, 13565-905 São Carlos, SP, Brazil
[b] Division of Mechanical Engineering, Technological Institute of Aeronautics, Praça Marechal Eduardo Gomes, 50. Vila das Acácias, 12228-900 São José dos Campos, SP, Brazil

ARTICLE INFO

Article history:
Received 5 January 2011
Received in revised form 4 February 2011
Accepted 8 February 2011
Available online 15 February 2011

Keywords:
Shape memory alloys
Fe–Mn–Si–Cr–Ni–(Co) shape memory stainless steel
Corrosion
Electrochemical techniques
Immersion tests

ABSTRACT

The corrosion behavior of three Fe–Mn–Si–Cr–Ni–(Co) shape memory stainless steels (SMSS) in 0.5 M H_2SO_4 solution was studied through electrochemical and immersion tests. The test results were compared with that of a type 304 (SS 304) austenitic stainless steel. The three SMSSs exhibited a passive behavior in 0.5 M H_2SO_4 solution; however, their anodic behavior in the active dissolution region was markedly different. The passive current densities of the SMSSs were similar to that of SS 304, although the critical anodic current required for passivation was higher. The corrosion rate of the SMSSs was much higher than that of SS 304. It was observed that the amount of Cr and Mn plays an important role in the corrosion behavior of SMSSs. The best corrosion behavior in acid media was shown by the SMSS that contained the highest amount of Cr and the lowest amount of Mn.

1. Introduction

Since the discovery of the shape memory effect (SME) in Fe–Mn–Si alloys by Sato et al. [1] in 1982, this new class of materials has attracted increasing attention due to its low production cost, excellent workability and good weldability in comparison to the traditional Ti–Ni and Cu-based shape memory alloys (SMAs) [2–4]. In the Fe–Mn–Si SMAs, the austenite (FCC structure) transforms into ε-martensite (HCP structure) during deformation ($\gamma \rightarrow \varepsilon$), and undergoes the reverse transformation into austenite upon heating ($\varepsilon \rightarrow \gamma$) to produce the SME. However, the corrosion resistance of these alloys is relatively poor, and reported recoverable strains without any treatment are usually less than about 2% [5,6]. In order to develop these Fe–Mn–Si SMAs, much effort has focused on improving the SME and the corrosion resistance. In this context, additions of chromium (Cr), nickel (Ni), cobalt (Co) and other elements to the Fe–Mn–Si SMAs have been accomplished successfully, resulting in an improvement in the SME and corrosion resistance [7–10]. The newly developed Fe–Mn–Si–Cr–Ni–(Co) SMAs are called shape memory stainless steels (SMSS) and are suitable for constrained recovery applications in various industrial sectors such as the chemical, petrochemical and construction industries. Liu et al. [11] and Li et al. [12] reported the successful application of SMSSs in joints for oil pipes.

Considering all these potential applications, the corrosion behavior is an important parameter for investigation, particularly the generalized corrosion attack occurring in acid media, due to the aggressive environments where these alloys are used. Furthermore, the literature contains very few studies about the corrosion behavior, corrosion rate, and anodic behavior in acid media of these new materials. Therefore, the aim of this work is to investigate the corrosion behavior of three SMSSs in 0.5 M H_2SO_4 solution, based on electrochemical and immersion tests.

2. Materials and methods

The SMSSs were prepared according to the following steps: (1) melting in a vacuum induction furnace (VIM), (2) hot forging at 1280 °C into a bar shape, (3) solution treating at 1050 °C for 1 h, and (4) quenching in a water bath at room temperature (25 °C). Table 1 shows the chemical composition of the SMSSs. Si, Mn, Cr, Ni and Co were determined by inductively coupled plasma optical emission spectrometry (ICP–OES). C was determined by pyrolysis using a LECO CS–444.

Cylindrical samples for the electrochemical tests were machined carefully and mounted in polyester resin after the electric contact, with special care taken to prevent the presence of crevices. The exposed area was 1.0 cm^2. Before the potentiodynamic and linear polarization measurements, the samples were wet ground with #600-grit silicon carbide (SiC) paper, washed in distilled water, and immersed in the electrochemical cell. The samples were then subjected to open circuit conditions until a steady state potential was reached. This procedure was accomplished in 30 min and the potential value obtained was considered the corrosion potential (E_{corr}).

All the electrochemical measurements were taken in 0.5 M H_2SO_4 solution prepared with analytical grade chemicals and distilled water. The solution was naturally aerated and the temperature was held at 25 °C. A conventional electrochemical cell was used, consisting of a platinum counter electrode and a saturated calomel reference electrode (SCE) connected to a potentiostat (Solartron 1287A).

* Corresponding author. Tel.: +55 16 33518507; fax: +55 16 33518258.
E-mail addresses: carlosdrovere@hotmail.com, carlosdrovere@gmail.com (C.A.D. Rovere).

0925-8388/$ – see front matter © 2011 Elsevier B.V. All rights reserved.
doi:10.1016/j.jallcom.2011.02.051

Table 1
Chemical composition (mass %) of the SMSSs.

Alloy	C	Si	Mn	Cr	Ni	Co	Fe
SMSS A	0.008	5.30	14.19	8.81	4.65	–	bal.
SMSS B	0.006	5.31	10.34	9.92	4.87	–	bal.
SMSS C	0.009	5.25	8.26	12.80	5.81	11.84	bal.

The potentiodynamic polarization measurements were carried out at sweep rates of 1 mV/s, starting from a potential of 200 mV below E_{corr}, to a potential of 1200 mV_{SCE}. Scanning electron microscopy (SEM) images were recorded after the polarization measurements. To obtain clear and detailed images, a mechanical polishing up to 1 μm (mirror finish) was performed before the polarization measurement.

The linear polarization measurements were carried out at sweep rates of 0.1667 mV/s in a range of ±10 mV with respect to E_{corr}. The polarization resistance (R_p) was converted to corrosion rate in millimeters per year (R_{mpy}), according to Eqs. (1) and (2) [13]:

$$R_{mpy} = \frac{0.13002 \times i_{corr} \times E_w}{\rho} \quad (1)$$

$$i_{corr} = \frac{\beta_\alpha \times |\beta_c|}{2.3R_p \times (\beta_\alpha + |\beta_c|)} \quad (2)$$

where i_{corr} is the corrosion current density (μA/cm²), E_w is the equivalent weight (chemical) of the alloy calculated according to the ASTM G102–89(2010) standard, ρ is the density of the alloy (g/cm³), R_p is the polarization resistance (Ω cm²), β_a (mV) and β_c (mV) are the anodic and cathodic Tafel slopes, respectively. The Tafel slopes were obtained by linear fitting of the potentiodynamic polarization data within ±50 to ±100 mV of the E_{corr}. Table 2 shows the density and equivalent weight of the alloys.

The stability of the anodic passive film was evaluated in open circuit conditions, based on the potential decay as a function of time. The anodic passive film was grown according to the following procedure: (1) the samples were mechanically polished up to 1 μm, (2) cathodically polarized at −800 mV_{SCE} for 5 min to remove the air-formed oxides, and (3) passivated at a constant potential of 500 mV_{ECS} for 1 h.

Immersion tests were carried out in a 0.5 M H_2SO_4 solution at 25 °C for 96 h, according to the ASTM G31–72(2004) standard. The samples were weighed at intervals of 24 h and the weight loss was calculated based on the difference in the samples' mass before the test (0 h) and after 24 h, up to 96 h. SEM images were recorded after 96 h of immersion.

To compare the corrosion behavior of the SMSSs with that of a standard corrosion resistant alloy, samples of type-304 (SS 304) austenitic stainless steel were solution treated at 1050 °C for 1 h, quenched in water bath and used in the electrochemical and immersion tests.

3. Results and discussion

Fig. 1 shows the potentiodynamic polarization curves of the SMSSs and SS 304 in 0.5 M H_2SO_4 solution. Note that the SMSSs and SS 304 show a similar active to passive transition behavior. The two materials showed the same transpassive breakdown potential; however, the anodic behavior of the alloys was very different in terms of the E_{corr}, the critical anodic current density required for passivation (i_{crit}), the primary passive potential (E_{pp}), and the passive potential range.

Table 3 presents the different electrochemical parameters determined from the potentiodynamic polarization curves. Note that the E_{corr} of the SMSSs is lower than that of the SS 304, indicating that the SMSSs are more active in the acid media than the SS 304. The i_{crit} of the SMSSs was also found to be higher than that of the SS 304 (3.46×10^{-4} A/cm²). Thus, the high i_{crit} values of the SMSSs indicate a greater difficulty to form passive film when compared to SS 304. This behavior can be attributed to the lower Cr content in the SMSSs [14]. On the other hand, the passive current density (i_{pass}) values are close to that of SS 304, indicating that the protectiveness of the passive films formed on SMSSs is similar to that of SS 304. It should be noted that the protectiveness of the passive films formed on the SMSSs is fairly high considering the low Cr content in these alloys. As Maji et al. [15] and Moriya et al. [16] suggested, this behavior may be related to the addition of Si (about 5–6%); however, the influence of Si on corrosion resistance has not yet been confirmed.

Table 2
Density and equivalent weight of SMSSs and SS 304.

Alloy	ρ (g/cm³)	E_w
SMSS A	7.51	23.04
SMSS B	7.52	22.93
SMSS C	7.63	22.76
SS 304	7.94	25.12

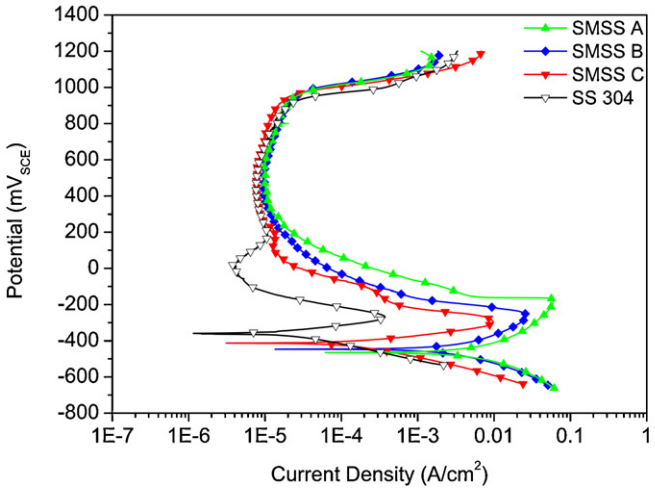

Fig. 1. Potentiodynamic polarization curves obtained from SMSSs and SS 304 in 0.5 M H_2SO_4 solution.

Fig. 2 shows the microstructures of the SMSSs after the potentiodynamic polarization test. A general corrosion attack can be observed in all the SMSSs; however, SMSS A exhibited the most severe attack, with intense corrosion clearly identifiable along the stacks of ε-martensite plates. A less pronounced corrosion attack was observed on SMSS C, followed by SMSS B.

To investigate the stability of the passive film grown anodically, the time (T_d) required for the onset of potential decay from the passive to the active state in the SMSSs was measured and compared with that of SS 304. According to Zhang et al. [17], T_d is a suitable parameter for the indication of passive film dissolution, and hence, its stability. Fig. 3 shows the potential decay curves (in open circuit conditions) of the SMSSs and SS 304 as a function of time. The curves for the SMSSs can be divided into three regions: (1) a region with a rapid potential drop; (2) a region showing an almost linear decrease, in which a slight potential variation over time is visible; and (3) a sudden fall in potential towards the E_{corr} value. Between regions 2 and 3 it is possible to obtain the Flade potential (E_F). This potential characterizes the dissolution of the passive film that was previously grown. The arrows in Fig. 3 indicate the E_F as well as the T_d. Moreover, it can be observed that the T_d values of the SMSSs are lower than that of SS 304, indicating the lower stability of the passive film grown anodically on SMSSs. Among the SMSSs, SMSS C exhibited the highest value of T_d (347 s) and the lowest E_F (−108.72 mV_{ECS}). The worst behavior was shown by SMSS A, in which the T_d and E_F remained at 143 s and 13.16 mV_{ECS}, respectively.

Table 4 shows the polarization resistance (R_p), corrosion current density (i_{corr}), and corrosion rate (R_{mpy}) obtained from the linear polarization measurements. Note that the i_{corr} and R_{mpy} of the SMSSs are much higher than that of SS 304, indicating that the corrosion resistance of these alloys is lower in acid media. Among the SMSSs, SMSS C showed the lowest R_{mpy} value (55.99 mpy) and

Table 3
Electrochemical parameters in 0.5 M H_2SO_4 solution.

Alloy	E_{corr} (mV_{ECS})	β_a (mV_{ECS})	$\lvert\beta_c\rvert$ (mV_{ECS})	E_{pp} (mV_{ECS})	i_{crit} (10^{-4} A/cm^2)	i_{pass} (10^{-6} A/cm^2)
SMSS A	−463.59	162.17	144.68	−187.86	548.10	8.95
SMSS B	−444.76	108.23	151.66	−268.52	226.63	7.38
SMSS C	−416.90	53.92	95.51	−297.53	76.05	5.74
SS 304	−356.48	62.22	90.11	−265.64	3.46	3.00

SMSS A the highest (1993.48 mpy). These results are in agreement with previous studies [18,19] and indicate that the Cr and Mn contents exert a significant influence on the corrosion resistance of SMSSs.

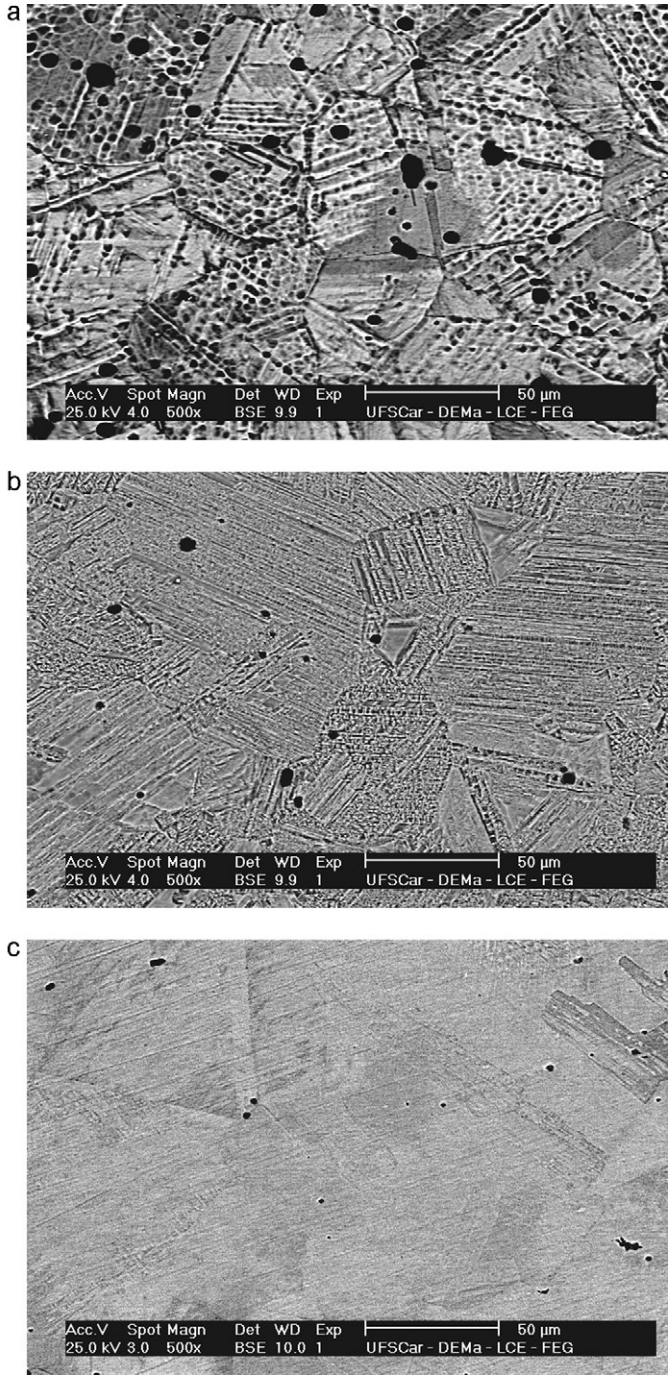

Fig. 2. SEM micrographs of SMSS microstructures after potentiodynamic polarization tests in 0.5 M H_2SO_4 solution: (a) SMSS A, (b) SMSS B and (c) SMSS C.

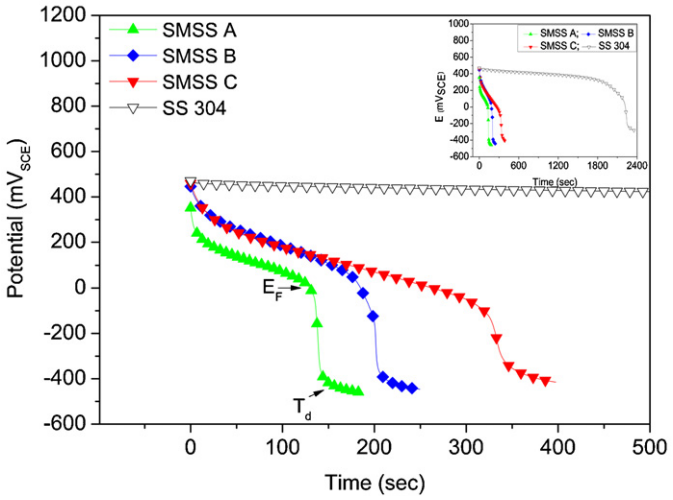

Fig. 3. Potential decay of SMSSs and SS 304 as a function of time after anodic passivation at 500 mV_{SCE} for 1 h in 0.5 M H_2SO_4 solution.

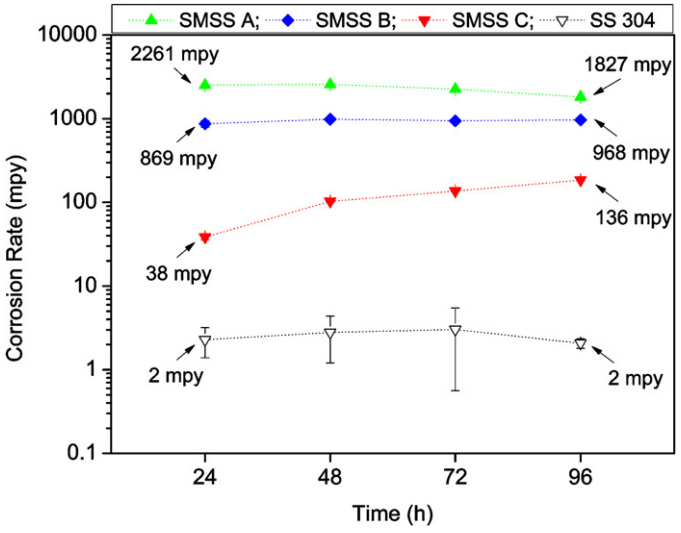

Fig. 4. Corrosion rate of SMSSs and SS 304 as function of immersion time in 0.5 M H_2SO_4 solution.

Fig. 4 shows the corrosion rates as a function of time for the immersion tests in 0.5 M H_2SO_4 solution. As can be seen, the R_{mpy} values obtained from the immersion tests are consistent with the R_{mpy} values obtained from the linear polarization measurements. These results indicate that the corrosion rates determined by the

Table 4
Polarization resistance (R_p) and corrosion rate (R_{mpy}) in 0.5 M H_2SO_4 solution.

Alloy	R_p (Ω cm^2)	i_{corr} (A/cm^2)	R_{mpy} (mpy)
SMSS A	6.62	5.03×10^{-3}	1993.48
SMSS B	10.31	2.56×10^{-3}	1048.30
SMSS C	103.21	1.45×10^{-4}	55.99
SS 304	774.19	2.07×10^{-5}	8.51

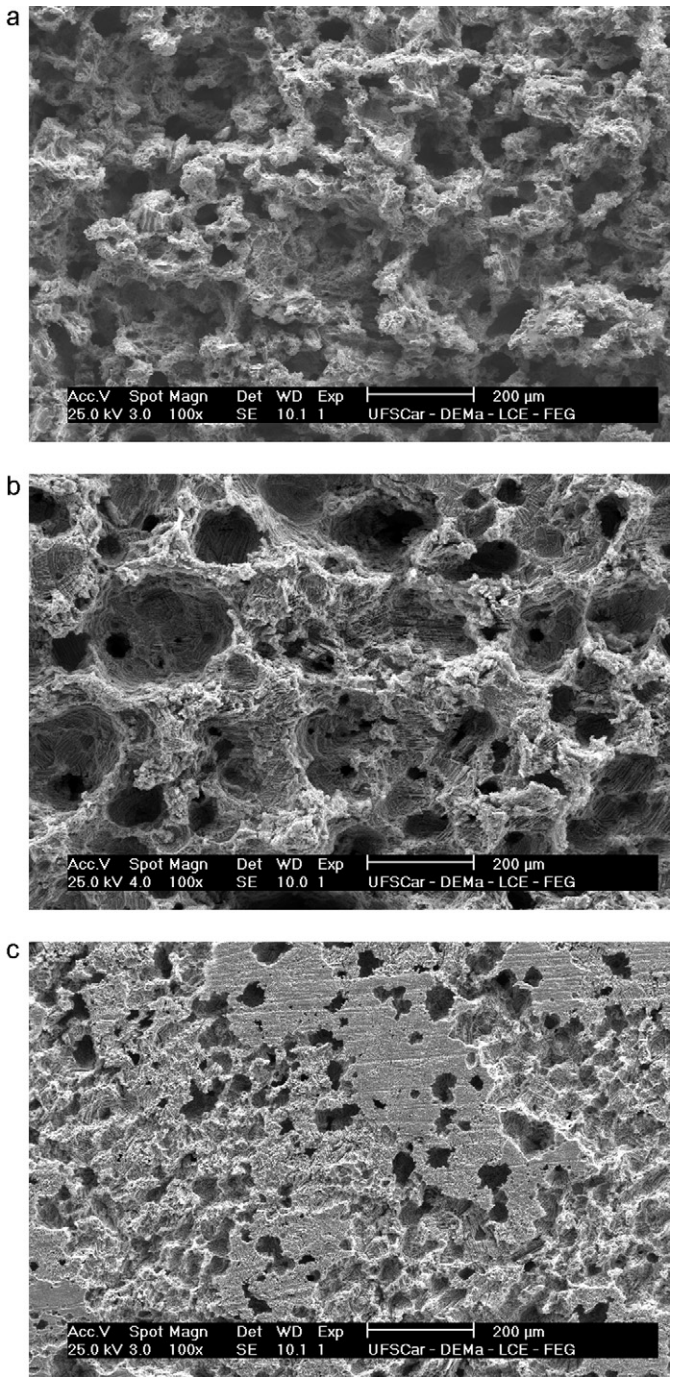

Fig. 5. SEM micrographs of the surface morphology of SMSS alloys after 96 h of immersion in 0.5 M H_2SO_4 solution: (a) SMSS A, (b) SMSS B and (c) SMSS C.

linear polarization technique represent a good approximation of the real corrosion rates determined from the immersion tests. However, the advantage of the linear polarization technique is that it saves time. On the other hand, it was found that the R_{mpy} values of the SMSSs were significantly higher than that of the SS 304. No significant change in the R_{mpy} values of the alloys was observed after longer exposure times except for SMSS C. Thus, the orders of R_{mpy} values for the alloys are SMSS A > SMSS B $\gg$ SMSS C $\gg$ SS 304.

Fig. 5 shows the surface morphology of the SMSSs after 96 h of immersion in 0.5 M H_2SO_4 solution. Note that the SMSSs exhibit an intense corrosion attack with a crater-like morphology over the entire microstructure. The SEM micrographs confirm the corrosion rate levels (R_{mpy}), with a significant corrosion attack visible in SMSS A, followed by SMSS B and C. Grajcar et al. [20] and Kannan et al. [21] observed similar surface morphologies in samples of high-manganese austenitic steels after immersion in H_2SO_4 solution. This morphology was attributed to the high corrosion rate promoted by the dissolution of Mn and Fe in acid solutions, and to the resulting strong cathodic reaction of hydrogen evolution.

A comparison of the corrosion performance of the SMSSs in 0.5 M H_2SO_4 solution indicates that the results of immersion and electrochemical tests follow the same tendency and that the balance between the Cr and Mn contents plays an important role in the corrosion behavior.

The opposite effect of Cr increase and Mn decrease among the SMSSs led to a shift in the E_{corr} values in the noble direction, with a consequent decrease in the corrosion rate (R_{mpy}). The same behavior was observed for the parameters T_d and i_{crit} with respect to changes in the Cr and Mn contents. According to Zhang and Zhu [22], the detrimental effect of Mn on the corrosion behavior is related to its low passivity coefficient and also to the formation of unstable Mn oxides. Wu et al. [23] attributed the negative effect of Mn to its strong chemical activity, i.e., low electronegativity, wide ranges of pH and potential in which Mn^{2+} ions are stable on the Pourbaix diagram, a high negative value of the standard electrode potential, and a high tendency to form nonmetallic inclusions. Park and Kwon [24] recently suggested that Mn facilitates the dissolution of Fe–Cr alloys by increasing the activity of Fe-adsorbed intermediates or by producing secondary intermediate species, which act as another dissolution pathway. The authors also suggested that Mn hinders the passivation process in acid solution by reducing the activity of Cr-adsorbed species. On the other hand, the beneficial effect of Cr in promoting the formation of a compact Cr_2O_3 film is well established. This oxide film protects the substrate by reducing its dissolution when in contact with an aggressive environment.

It is interesting to mention that the Cr and Mn contents also affect the SME of SMSSs. Moreover, the addition of Mn is essential to obtain the SME in Fe-based SMAs [7,19,25]. Hence, taking into account that the SMSSs exhibited an unacceptably high corrosion rate in the corrosion potential region, it is possible to state that this new type of stainless steel is suitable for application in highly oxidizing environments or under conditions of anodic protection.

4. Conclusions

Based on the results of the electrochemical and immersion tests of the SMSSs in acid media, the following conclusions can be drawn:

1 The three SMSSs and the SS 304 showed a similar passive region; however, their anodic behavior in the active region of dissolution differed significantly.
2 The SMSSs alloys exhibited a low capacity to form passive films when compared to SS 304; however, the protectiveness of the anodically formed passive films was similar to that of SS 304.
3 The stability of the passive films formed anodically on the SMSSs was much lower than that formed on SS 304.
4 The corrosion rate of the SMSSs was much higher than that of SS 304.

Acknowledgements

The authors gratefully acknowledge PPGCEM/UFSCar (Postgraduate Program in Materials Science and Engineering of the Federal University of São Carlos) and the Brazilian research funding agency CNPq (National Council for Scientific and Technological Development) for their financial support of this work.

References

[1] E. Sato, K. Chishima, T. Soma Mori, Acta Metall. 30 (1982) 1177–1183.
[2] K. Otsuka, C.M. Wayman (Eds.), Shape Memory Materials, Cambridge University Press, Cambridge, 1988.
[3] S. Kajiwara, Mater. Sci. Eng. A 273–275 (1999) 67–88.
[4] H.C. Lin, K.M. Lin, Y.C. Chuang, T.S. Chou, J. Alloys Compd. 306 (2000) 186–192.
[5] H. Li, D. Dunne, ISIJ Int. 37 (1997) 605–609.
[6] D.F. Wang, Y.R. Chen, F.Y. Gong, D.Z. Liu, W.X. Liu, J. Phys. IV, Colloque C8 5 (1995) 527–530.
[7] H. Otsuka, H. Yamada, T. Maruyama, H. Tanahashi, S. Matsuda, M. Murakami, ISIJ Int. 30 (1990) 674–679.
[8] J. Otubo, P.R. Mei, S. Koshimizu, J. Phys. IV, Colloque C8 5 (1995) 427–432.
[9] H.B. Peng, Y.H. Wen, B.B. Ye, N. Li, Mater. Sci. Eng. A 504 (2009) 36–39.
[10] X. Huang, S. Chen, T.Y. Hsu, X. Zuyao, J. Mater. Sci. 39 (2004) 6857–6859.
[11] D.Z. Liu, D.F. Wang, W.Y. Ji, W.X. Liu, Proceedings of the 2nd International Conference on Shape Memory and Superelasitc Technologies, California, 1997, p. 329.
[12] J.C. Li, X.X. Lü, Q. Jiang, ISIJ Int. 40 (2000) 1124–1126.
[13] A.J. Sedriks, Corrosion of Stainless Steel, second ed., Wiley, New York, 1996.
[14] K. Osozawa, H.J. Engell, Corros. Sci. 6 (1966) 389–393.
[15] B.C. Maji, C.M. Das, R.K. Madangopal Krishnan, Ray Corros. Sci. 48 (2006) 937–949.
[16] Y. Moriya, H. Kimura, S. Ishizaki, S. Hashizume, S. Suzuki, H. Suzuki, T. Sampei, J. Phys. IV, Colloque C4 1 (1991) 433–437.
[17] Y.S. Zhang, X.M. Zhu, M. Liu, R.X. Che, Appl. Surf. Sci. 222 (2004) 89–101.
[18] X.M. Zhu, Y.S. Zhang, Corrosion 54 (1998) 3.
[19] O. Sö derberg, X.W. Liu, P.G. Yakovenko, K. Ullakko, V.K. Lindroos, Mater. Sci. Eng. A 273–275 (1999) 543–548.
[20] A. Grajcar, S. Kołodziej, W. Krukiewicz, Arch. Mater. Sci. Eng. 41/2 (2010) 77–84.
[21] M. Bobby Kannan, R.K. Singh Raman, S. Khoddam, Corros. Sci. 50 (2008) 2879–2884.
[22] Y.S. Zhang, X.M. Zhu, Corros. Sci. 41 (1999) 1817–1833.
[23] X.Q. Wu, S. Xu, J.B. Huang, E.H. Han, W. Ke, K. Yang, Z.H. Jiang, Mater. Corros. 59 (2008) 676.
[24] K. Park, H. Kwon, Electrochim. Acta 55 (2010) 3421–3427.
[25] M. Murakami, H. Otsuka, H.G. Suzuki, S. Matsuda, Proceedings of the International Conference on Martensitic Transformations (ICOMAT-86), Nara, 1986, p. 985.